ACS SENSORS

pubs.acs.org/acssensors

Article

Ratiometric Fluorescent Nanohybrid for Noninvasive and Visual Monitoring of Sweat Glucose

Yaoxuan Cui, Wei Duan, Yao Jin, Fangjie Wo, Fengna Xi,* and Jianmin Wu*

Cite This: *ACS Sens.* 2020, 5, 2096–2105

Read Online

ACCESS | Metrics & More | Article Recommendations | Supporting Information

ABSTRACT: Noninvasive and visual monitoring of glucose is highly desirable for diabetes diagnostics and long-term home-based health management. Owing to the correlation of the glucose level between blood and sweat, on-body sweat glucose detection provides potential for noninvasive healthcare but is highly challenging. Herein, we for the first time demonstrate a wearable skin pad based on the ratiometric fluorescent nanohybrid, which can realize noninvasive and visual monitoring of sweat glucose. Luminescent porous silicon (PSi) particles, which have a porous structure and oxidation-responsive photoluminescence decay, are chosen to load (adsorb or entrap) carbon quantum dots (CQDs) for the construction of the dual fluorescence nanohybrid. Bimetallic (Au and Ag) nanoparticles (BiM) are also co-decorated on the PSi particle to improve detection sensitivity by enhancing PSi's initial fluorescence and oxidation kinetics. Owing to the efficient fluorescence resonance energy transfer effect, BiM-CQDs@PSi initially exhibits PSi's red fluorescence with complete quenching of CQDs's blue fluorescence. The oxidation of PSi triggered by hydrogen peroxide (H_2O_2) weakens the FRET effect and decays PSi's fluorescence, causing ratiometric fluorescence to change from red (PSi) to blue (CQDs). A wearable skin pad is easily fabricated by co-immobilization of BiM-CQDs@PSi and glucose oxidase (GOX) in a transparent and biocompatible chitosan film supported by an adhesive polyurethane membrane. When the skin pad is attached on the body, the same ratiometric fluorescence transition (red → blue) is observed upon the stimulation of H_2O_2 generated in GOX-catalyzed oxidation of sweat glucose. Based on the strong correlation between the ratio of the fluorescence change and sweat glucose level, clinical tests toward diabetics and healthy volunteers can clearly indicate hyperglycemia.

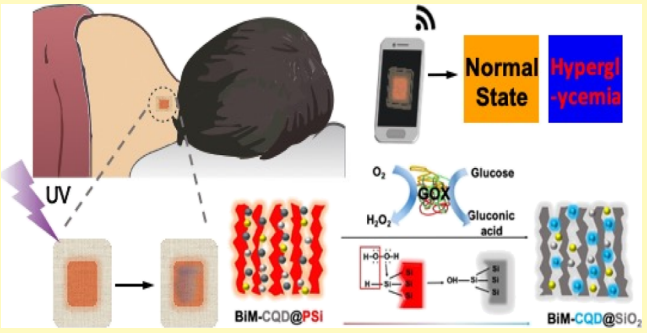

KEYWORDS: *noninvasive monitoring, visual sensor platform, sweat glucose, porous silicon, carbon quantum dots*

Diabetes is one of the most popular chronic diseases around the world and seriously threatens human health. To prevent severe complications (*e.g.*, cardiovascular diseases, kidney failure, blindness, and nerve degeneration), frequent blood glucose (BG) checks in daily life are essential for diabetic patients.[1,2] However, conventional commercial glucometers involve invasive and repetitive finger-stick blood tests which bring physical pain, psychological stress, and risk of wound infection.[3] Noninvasive and wearable sensors with on-body, continuous, and visual glucose monitoring are highly desirable for predictive clinical diagnosis and personalized health care.[4,5]

As an alternative to blood, easily accessible human biofluids (*e.g.*, sweat,[6,7] skin interstitial fluid,[8] tears,[9] saliva,[10] and urine[11]) provide potential capability for noninvasive analysis of biomarkers that reflect insightful physiological information of body. It has been proven that glucose in these biofluids is diffused from blood vessels through endothelium or glands,[12] and its concentration is linearly correlated with that in blood.[13−16] Owing to easy access, sweat provides advantage of continuous sampling on various body areas (*e.g.*, arm, wrist, neck, and forehead).[17,18] However, direct monitoring of sweat glucose remains a great challenge because the sweat glucose level is ∼100 times lower than the BG level.[19] Detection sensitivity is the crucial issue that must be addressed.

Comparing to other sensing modalities (*e.g.*, electrochemical sensors), fluorescent (FL) sensors have attracted considerable interests owing to high sensitivity, simple operation, fast or real-time monitoring, and visual readout. Most FL sensors only rely on one FL probe with particular emission wavelength, which can be easily influenced by different factors (*e.g.*, the intensity of excitation light, concentration of probe, and environmental interference).[20,21] Alternatively, the ratiometric FL system based on the ratio of two different emission is less prone to be affected, leading to high sensitivity, good accuracy, and visualized presentation.[22,23] However, the commonly used

Received: April 8, 2020
Accepted: May 26, 2020
Published: May 26, 2020

https://dx.doi.org/10.1021/acssensors.0c00718
ACS Sens. 2020, 5, 2096–2105

FL materials [*e.g.*, organic molecules and semiconductor quantum dots (QDs)] often suffer from high cost and low biocompatibility. Hence, visual sensing using the ratiometric FL hybrid based on cheap and environmentally friendly FL probes is needed.

Luminescent porous silicon (PSi) promises a wide range of biomedical applications owning to the unique combination of key merits including high loading capacity originated from abundant pore structure, tunable fluorescence, high degradability, excellent biocompatibility, easy preparation, and low cost.[24−26] Several works have revealed the strong dependence of its fluorescence properties on surface chemistry, especially its oxidation state.[27] For instance, our previous work revealed that the elevated reactive oxygen species level in the skin wound can trigger the oxidation of PSi and result in a thicker SiO_2 layer, which lead to fluorescence decay of PSi and also block the fluorescence resonance energy transfer (FRET) effect between PSi and the carried drug (ciprofloxacin, an antibacterial drug with blue fluorescence).[25] This stimuli-responsive fluorescence possesses great potential for versatile platforms of the ratiometric FL system and visual monitoring. The nanohybrid structure based on PSi decorated with QDs including carbon QDs (CQDs)[28,29] or semiconductor QDs (*e.g.*, CdS and PbS QDs)[30−32] have displayed superior optical properties including the amplificated photoluminescence (PL) signal of QDs or two-mode optical sensing capacity based on PL of QDs and Bragg reflectivity of PSi. As a member of the nanocarbon family, CQDs demonstrate advantages of biocompatibility (depending on their synthesis), facile synthesis, high brightness, and good stability.[33] Thus, the nanohybrid structure based on PSi decorated with CQDs has great potential in bioassay.

In this work, we for the first time demonstrate noninvasive and visual monitoring of sweat glucose using wearable skin pad based on the ratiometric FL nanohybrid. CQDs are decorated on the porous structure of PSi particles, leading to dual FL nanohybrid (CQDs@PSi). To improve the detection sensitivity toward sweat glucose, bimetallic nanoparticles (BiM) including gold nanoparticles (AuNPs) and silver nanoparticles (AgNPs) are co-modified on PSi to enhance its initial fluorescence intensity and catalyze the PSi oxidation triggered by hydrogen peroxide (H_2O_2). A wearable skin pad could be easily fabricated by co-immobilization of the as-prepared BiM-CQDs@PSi and glucose oxidase (GOX) in a transparent and biocompatible chitosan (CS) film supported by an adhesive polyurethane (PU) membrane. Owing to the FRET effect between PSi and CQDs, blue fluorescence of CQDs is quenched and the skin pad initially shows red fluorescence of PSi. When the skin pad is attached on the body, H_2O_2 generated in GOX-catalyzed sweat glucose oxidation will promote the oxidation of PSi, thus leading to the decay of PSi's fluorescence and the recovery of CQDs's fluorescence, making fluorescence change from red (PSi) to blue (CQDs). In addition, the kinetics of this visual fluorescence change (red→blue) is proportional to the concentration of sweat glucose. Using photos taken by the smartphone, simple data processing is developed and clinical test toward diabetics and healthy volunteers is easily realized. The developed noninvasive and visual monitoring system of sweat glucose can clearly indicate hyperglycemia through the clinical test, showing great potential in daily healthcare.

EXPERIMENTAL SECTION

Preparation of Luminescent Porous Silicon Particles. PSi was etched from anodization of a boron-doped silicon wafer (resistivity: 0.0005−0.0012 Ω/cm) with a [100] crystal orientation in an electrolyte mixture of hydrofluoric acid (HF) aqueous (48% by mass, Alatin Corp.) and ethanol (v/v = 4:1). The electrochemical etching was conducted under a constant current density of 77 mA/cm^2 for 600 s. Then, the PSi layer was removed from the Si substrate by application of a current density of 22 mA/cm^2 for 180 s in an ethanol solution of 3.3% HF. To obtain luminescent PSi particles, the PSi film was immersed in phosphate-buffered saline (PBS) solution (0.1 M, pH = 7.4) for 12 h to activate the luminescence emission and then washed with deionized water for three times. The luminescent PSi film was placed in deionized water and fractured into particles by ultrasonication (400 W) for 15 min.

Modification of PSi Particles with AuNPs and AgNPs. AuNPs were prepared by the traditional Frens's synthesis with chloroauric acid ($HAuCl_4$) and citrate sodium.[34] Briefly, aqueous of $HAuCl_4$ (15 mM) was heated to boiling (100 °C) before citrate sodium aqueous solution (0.1 M) was added ($V_{HAuCl_4}/V_{citrate\ sodium}$ = 25:1). The temperature was maintained for 30 min to get the dark red solution of AuNPs. AgNPs were prepared by the reduction of $AgNO_3$ (1 mM) with glucose (10 mM) in NaOH (1 M) and ammonia (14.7 M) medium ($V_{AgNO_3}/V_{glucose}/V_{NaOH}/V_{ammonia}$ = 100:100:1:1) for 30 min at room temperature.[35] To modify AuNPs and AgNPs to porous Si, the mixture solution of PSi, AuNPs, and AgNPs were shaken for 1 h. Then, the obtained BiM loaded PSi particles (BiM@PSi) were centrifuged (8000 rpm, 5 min) followed by a thorough rinse with deionized water.

Preparation of CQDs@PSi and BiM-CQDs@PSi Composite Particles. According to the previous method, CQDs were prepared by a one-step low-temperature solid-phase approach.[33] Briefly, urea and sodium citrate were mixed with a molar ratio of 6:1and then heated at 180 °C for 1 h. After the pH value of the obtained CQDs aqueous was adjusted to 4 with HCl (1 mM), CQDs were loaded into PSi particles by mechanical shaking of PSi in CQDs aqueous for 5 h, and the obtained CQDs@PSi particles were isolated from solution by centrifugation (8000 rpm, 5 min) followed with thorough rinsing with deionized water to remove unloaded CQDs. Similarly, BiM-CQDs@PSi particles were obtained by mechanical shaking of BiM@PSi in CQDs aqueous, followed with the centrifugation and rinsing.

Construction of the Flexible BiM-CQDs@PSi/GOX/CS/PU Pad. To prepare wearable pad for noninvasive analysis, BiM-CQDs@PSi and GOX were co-immobilized in the CS film supported by a sticky PU membrane (3M, USA). Briefly, BiM-CQDs@PSi particles were dispersed in CS solution (1%) and GOX solution (1 mg/mL), and then, 3-glycidyloxypropyl-trimethoxysilane (GPTMS, 3%) was added to the solution to form a cross-linked polymer gel. Before the gel cross-linked, the mixture solution (50 μL) was dropped to the PU film (0.6 × 0.6 cm^2). Then, a thin film was formed at the PU membrane surface after 2−3 h at room temperature.

Characterization. Transmission electron microscopy (TEM) images of PSi, CQDs, BiM@PSi, CQDs@PSi, and high-angle annular dark field−scanning TEM (HAADF−STEM) image of BiM-CQDs@PSi particles were obtained from JEM-1010 (Japan Electronics, Japan) at an operating voltage of 100 kV. The absorbance spectra of PSi particles, CQDs@PSi particles, AuNPs, and AgNPs were measured with the SP-756PC UV−VIS spectrometer (Shanghai Spectrum, China). The diffuse reflection-FTIR spectra of PSi particles after different oxidation stages by H_2O_2 were detected by diffuse reflection-infrared Fourier transform spectroscopy (NICOLET iS10, Thermo Scientific, USA). The elements on the surface of PSi and BiM@PSi particles were analyzed by the X-ray photoelectron spectrophotometer (VG ESCALAB MKII, VG Scientific, UK). The Si degradation dynamics of PSi and BiM@PSi particles were measured by inductively coupled plasma optical emission spectrometry (ICP−OES, ICP6000, Thermo Scientific, USA). Briefly, 90 mg of PSi particles was used to prepare BiM@PSi particles. Then, the obtained BiM@PSi and 90 mg of PSi particles were incubated in 6 mL H_2O_2 solution (100 μM, PBS,

https://dx.doi.org/10.1021/acssensors.0c00718
ACS Sens. 2020, 5, 2096−2105

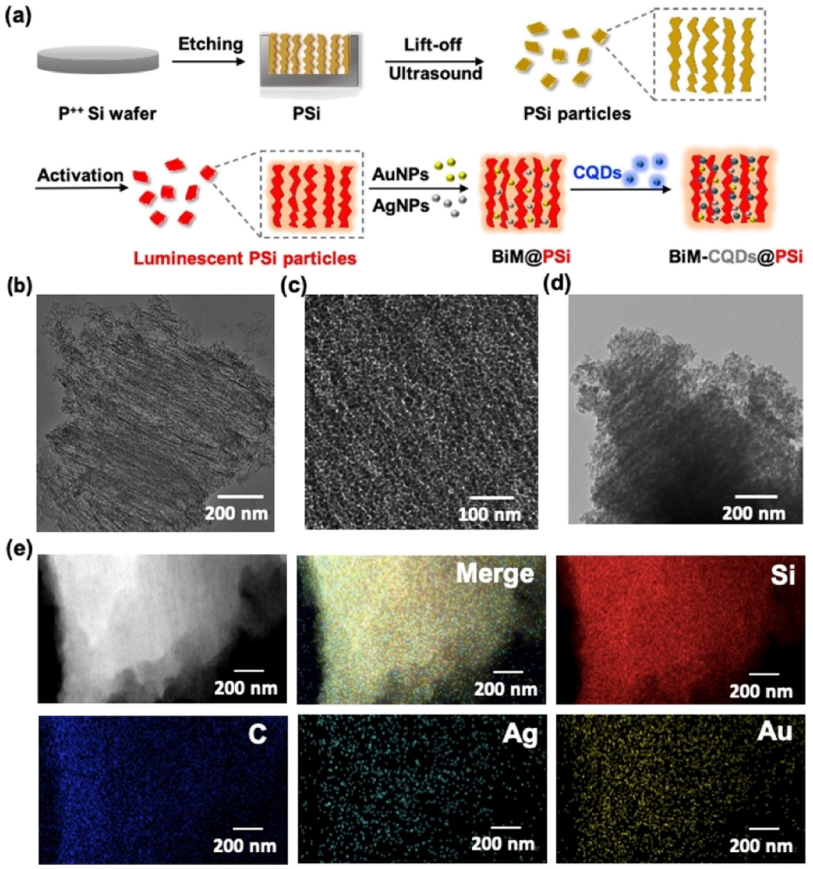

Figure 1. (a) Schematic illustration for the preparation of BiM-CQDs@PSi particles. (b,c) TEM images of PSi particles. (d) TEM image of BiM@PSi particles. (e) HAADF−STEM image and merge elements, Si, C, Au, Ag element mapping images of BiM-CQDs@PSi particles.

pH = 7.4) at 37 °C, respectively. Then, an aliquot (200 μL) of the supernatant was diluted with deionized water to 15 mL, and the pH value was adjusted to 5.0 by 0.1 M HCl. The amount of Si elemental in the supernatants was measured by ICP−OES, and the spectrometer was calibrated at the position of 2p line of Si at a binding energy of 99.15 eV. The FL spectra were acquired by a fiber spectrometer (QE pro, Ocean optics) with a 365 nm UV excitation. The FL images were acquired by a fluorescence microscope (NE950, Nexcope, China) attached with a highly sensitive CCD detector (MC20-C).

Glucose Detection in GOX Medium. Simulated sweat aqueous consisted of NaCl (5%), urea (2%), lactic acid, and different contents of glucose. BiM-CQDs@PSi particles were incubated in simulated sweat aqueous contained different concentrations of glucose (0, 5, 7.5, 10, and 15 mM). The fluorescence spectra and images of BiM-CQDs@PSi particles incubated in simulated sweat aqueous were recorded under a fluorescence microscope. The R/B value was analyzed by Photoshop CC software.

Glucose Detection on Simulated Skin. Cotton pad is applied as simulated skin. The CQDs@PSi/GOX/CS/PU pad was attached on a piece of cotton pad and simulated sweat containing different levels of glucose was dropped on the back of the cotton pad. Then, the cotton pad was placed at a 37 °C heating panel, and the FL photo was acquired by a cellphone camera (iphone 6S, Apple Inc. USA) under a UV LED (λ_{ex} = 377 nm) irradiation. The R/B value was analyzed by Photoshop CC software.

On-Body Sweat Glucose Monitoring. A piece of the BiM-CQDs@PSi/GOX/CS/PU pad was patched on the back area of neck of the volunteer before sleep. The fluorescence photo was taken by the cell phone camera under a UV LED (377 nm) irradiation before and after sleep (10 h), and the fasting BG of each volunteer was recorded by the glucometer (Sannuo, GA-3, China) after the pad was removed.

Image Processing and Analysis. Every two fluorescence photos taken from the same people before and after patching were classified into one group; therefore, 24 groups of images were obtained. Red and blue channel intensity values of each pixel in all FL photos were extracted by the Open CV software. The R/B values were calculated and normalized within one group; thus, the experimental error from slight differences in the initial material can be avoided. Then, the maximum R/B value was defined as the red color and the minimum value was defined as the blue color, and other points are given corresponding colors between red and blue according to their respective R/B values. After that, processed new images are obtained, which demonstrated better distinguishability, and significant color difference caused by different glucose levels can be recognized. Furthermore, to achieve a more intuitive and standardized visual effect, the mean value of normalized R/B values of every image was calculated and colored from red to blue according to the numerical value. Finally, average colors of each image were obtained.

RESULTS AND DISCUSSION

Preparation and Characterization of Luminescent PSi and BiM-CQDs@PSi Particles. According to the method mentioned in our previous work,[25] the PSi film (a porosity of ∼64.2%, thickness of 22.9 μm, specific surface area of ∼561 m^2/g, and averaged pore diameter of 17.3 nm) was prepared using electrochemical etching (anodic oxidation) in mixed solution of HF and ethanol ($Si + 2h^+ + 6HF \rightarrow SiF_6^{2-} + H_2 + 4H^+$, Figure 1a).[36] Then, the freestanding porous Si film was electrochemically removed from the bulk wafer using anodic oxidation at lower concentrations of HF and current density. The following ultrasonic treatment led to the formation of PSi particles. The newly etched porous silicon did not possess

https://dx.doi.org/10.1021/acssensors.0c00718
ACS Sens. 2020, 5, 2096−2105

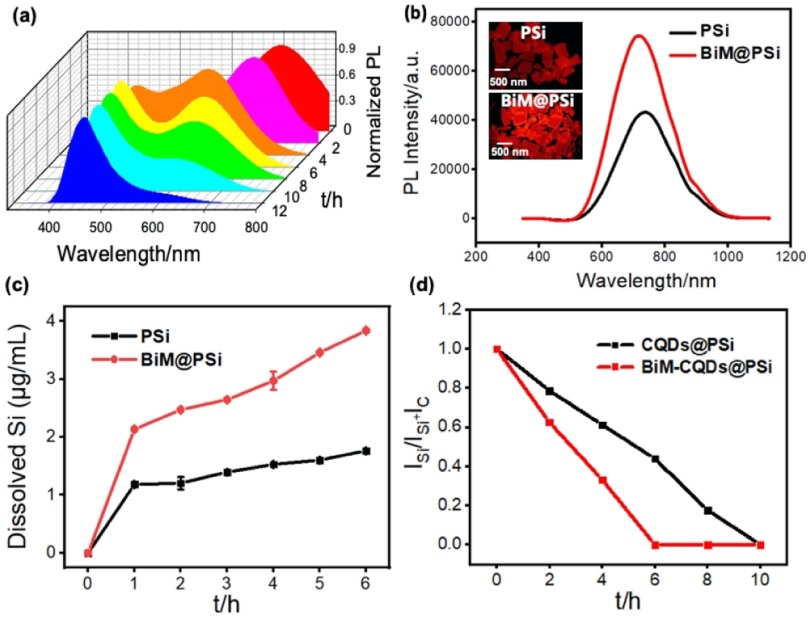

Figure 2. (a) Evolution of fluorescence emission spectra during incubation of CQDs@PSi in PBS medium. (b) Fluorescence emission spectra of PSi and BiM@PSi particles. Insets are the corresponding digital photos under UV irradiation (377 nm). (c) Releasing kinetics of Si species in the supernatant of PSi and BiM@PSi particle solution (100 μM H_2O_2 in PBS, pH = 7.4, 37 °C). (d) Ratiometric intensity of (I_{Si}/(I_{Si} + I_C) of CQDs@PSi (black) and BiM-CQDs @PSi (red) as a function of oxidation time in H_2O_2 solution (100 μM, PBS, pH = 7.4, 37 °C).

fluorescence. After activated in phosphate aqueous solution (pH = 7.4, 25 °C, 12 h), luminescent PSi particles with bright red luminescence were obtained owing to the passivation of nonradiative surface defects and generation of surface states by formation of SiO_2 thin layer through slight oxidation.[25] TEM images of the luminescent PSi (Figure 1b,c) indicated that the porous structure retained after the luminescence activation of the PSi particle.

The BiM-CQDs@PSi nanohybrid was prepared following the procedure illustrated in Figure 1a. The porous nature of PSi makes it a good carrier for the preparation of hybrid materials. As illustrated in Figure 1a, AuNPs (~13 nm)[34] and AgNPs (~14 nm)[35] could be easily loaded on PSi particles using simple mixing and shaking, leading to bimetallic nanoparticle-modified PSi (BiM@PSi). The as-prepared BiM@PSi particles still maintain porous morphology of PSi (Figure 1d). The appearance of characteristic plasma resonance absorption peaks of AuNPs (~513 nm)[37] and AgNPs (~388 nm)[38] in UV−vis absorption spectra (Figure S1 in Supporting Information) proves efficient composites of AuNPs and AgNPs in PSi nanoparticles, which can be further confirmed by peaks of Au 4f and Ag 3d in X-ray photoelectron spectroscopy (Figure S2 in Supporting Information). Mapping images of the energy -dispersive spectrum equipped in transmission electron microscope furtherly reveal the successful preparation of this multicomponent nanohybrid with CQDs, AuNPs, and AgNPs on the porous structure of PSi particles. As shown in Figure 1e, C signals from CQDs and Au and Ag signals from BiM are well distributed in Si signals from PSi, indicating a uniform structure of BiM-CQDs@PSi.

FRET Effect and Ratiometric Fluorescence between CQDs and PSi. Fluorescence analysis has advantages of high sensitivity, simple operation, visual signal, and direct monitoring *in vivo*. However, most FL sensors employ intensity change at a single emission peak, which can be easily influenced by variety of conditions (*e.g.*, excitation light intensity, probe concentration, and environmental interferences). As an alternative, ratiometric fluorescence probes conferred the sensors with higher accuracy based on the ratio of intensities at two different emission peaks. Furthermore, ratiometric fluorescence can provide a very intuitive color change and realize visual detection using human eyes. Owing to the excellent biocompatibility and good photoluminescence properties, PSi and CQDs are chosen to build dual-fluorescence nanohybrids by loading CQDs on the porous structure of PSi. CQDs with diameter ~10 nm (Figure S3) displays bright blue emission, and PSi shows red fluorescence under UV excitation (365 nm), as demonstrated in insets in Figure S4. The emission spectrum of CQDs with a maximum peak at 465 nm overlaps with the absorption spectrum of PSi in the range of 300−500 nm (Figure S4), suggesting possibility for FRET between the two FL materials. When CQDs are loaded in PSi, only red fluorescence from PSi was initially observed (peaked at ~700 nm) in PL spectra (Figure 2a) and images of the fluorescence microscope (Figure S5 in Supporting Information), indicating that the blue fluorescence of CQDs was completely quenched owing to the efficient FRET effect between PSi and CQDs. It is presumed that CQDs acted as the energy donor, while PSi was the acceptor owing to high density of electronic states and the large surface. Along with the oxidation and degradation process of PSi in PBS aqueous, the intensity of the red fluorescence peak (PSi, ~750 nm) decreased gradually, while the intensity of the blue fluorescence peak (CQDs, ~400 nm) increased gradually (Figure 2a), leading to ratiometric fluorescence change from red to blue. This change can be easily distinguished by the naked eye. As shown in Figure S5 in Supporting Information, the colors of CQDs@PSi appear from red (PSi) to pink (the mixture of red fluorescence from PSi and recovered blue fluorescence from CQDs. The earlier color change of PSi's edge part is attributed to faster oxidation. The mechanism for this ratiometric fluorescence lies in slow oxidation of PSi in

https://dx.doi.org/10.1021/acssensors.0c00718
ACS Sens. 2020, 5, 2096−2105

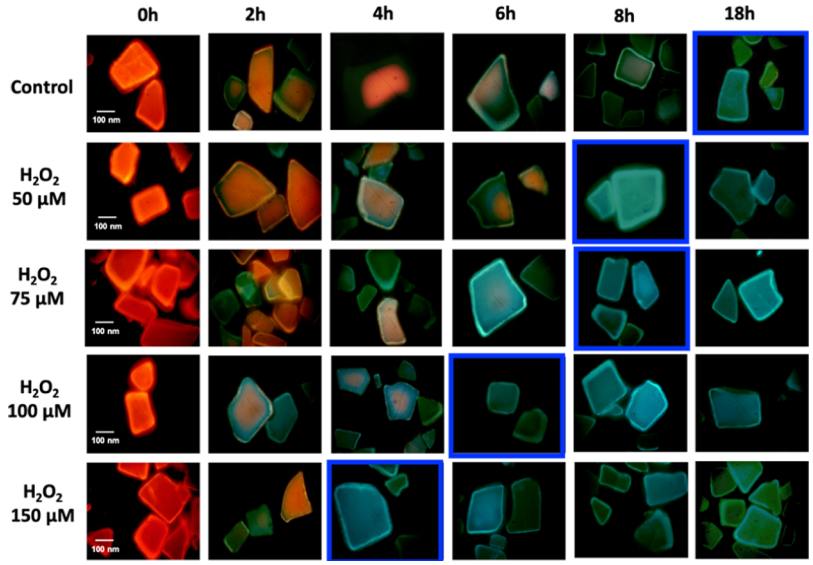

Figure 3. Fluorescence images of BiM-CQDs@PSi particles in simulated sweat aqueous with different concentrations of H_2O_2. Images with first appearance of complete blue fluorescence were marked by blue borders.

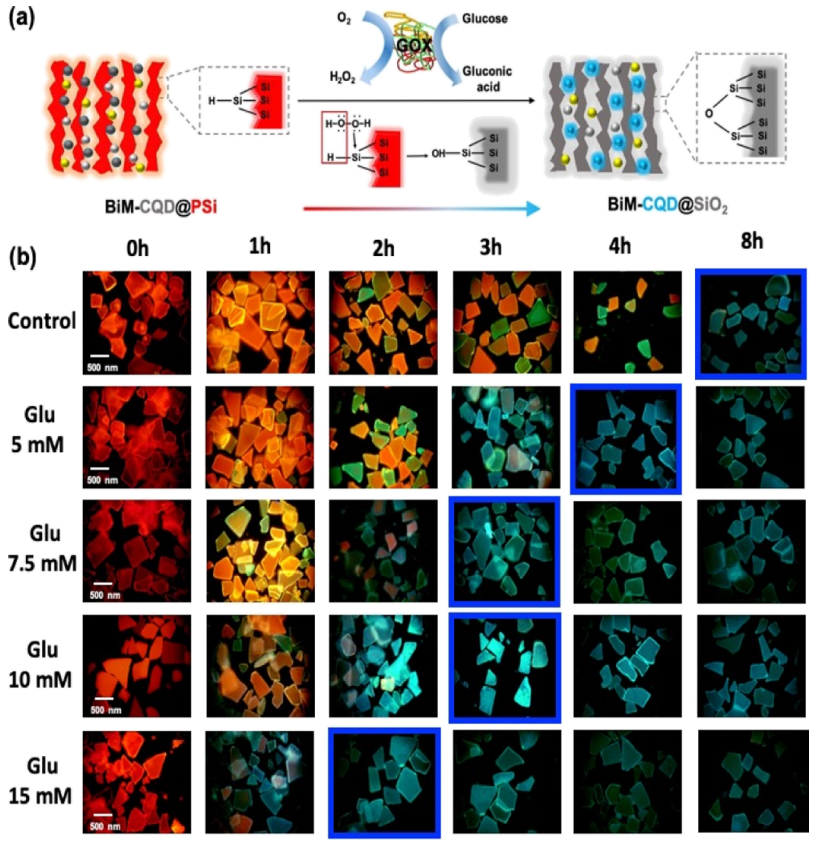

Figure 4. (a) Schematic illustration for glucose monitoring using ratiometric fluorescence of BiM-CQDs@PSi upon the stimulation of H_2O_2 generated in GOX-catalyzed oxidation of glucose. (b) Fluorescent images of BiM-CQDs@PSi particles in GOX solution with different concentrations of glucose. Images with first appearance of complete blue fluorescence were marked by blue borders.

aqueous solution. The formed SiO_2 insulator reduces density of free electronic states and concentration of the free carrier in PSi.[25,39] Thus, FRET between PSi and CQDs is weakened and the fluorescence of CQDs is recovered. At the same time, the eliminated quantum-confined Si domains and the generated defect energy level remarkably decreases red fluorescence of PSi. Taken together, CQDs@PSi nanohybrid exhibited visual fluorescence color changes.

Enhanced Fluorescence and Accelerated Oxidation of PSi in the BiM-CQDs@PSi Nanohybrid. In comparison with PSi particles, BiM@PSi shows obviously brighter red luminescence (insets in Figure 2b) with 82% increase of peak intensity in the emission spectrum (Figure 2b), indicating the

https://dx.doi.org/10.1021/acssensors.0c00718
ACS Sens. 2020, 5, 2096−2105

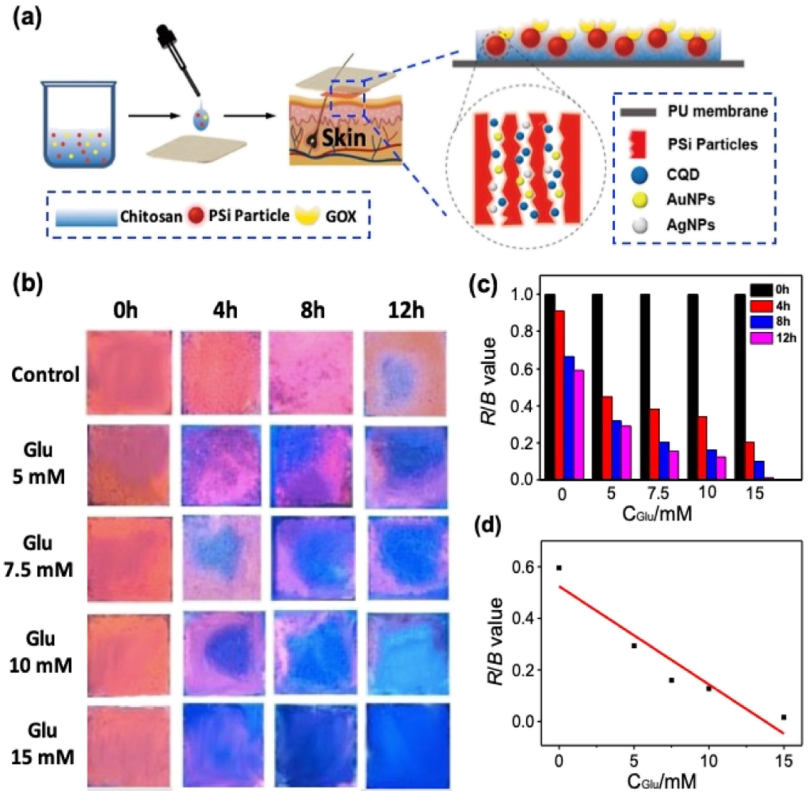

Figure 5. (a) Schematic illustration for the preparation of the wearable BiM-CQDs@PSi/GOX/CS/PU pad. (b) Fluorescent photos of the BiM-CQDs@PSi/GOX/CS/PU pad on simulated skin incubated with different concentrations of glucose. (c) *R*/*B* values of FL photos during incubation. (d) Correlation of *R*/*B* value and glucose concentration after incubation for 12 h.

sensitized fluorescence of PSi. This phenomenon may arise from resonant interactions between emission dipoles and localized surface plasmons positioned at a few nanometers from the AuNP or AgNP surface.[40] In addition, the enhancement of fluorescence by bimetallic nanoparticles is more significant than that caused by the corresponding single type of metal nanoparticle (66% or 14% increase of peak intensity in emission spectrum for AuNPs-PSi or AgNPs-PSi, respectively, Figure S6 in Supporting Information), suggesting a synergistic effect between AuNPs and AgNPs.

Hydrogen peroxide-triggered oxidation of PSi particles was further investigated because H_2O_2 is a vital component of reactive oxygen species in the biological system. When PSi particles were exposed to H_2O_2, the surface of PSi could be further oxidized. This oxidation process was revealed using diffuse reflectance FTIR spectroscopy (DR-FTIR). As shown in Figure S7 in Supporting Information, the signal of the Si−H bond gradually decreases accompanying with the gradual increase of the Si−O−Si signal, indicating the formation of the SiO_2 layer. The instability of the formed SiO_2 in aqueous solution [$SiO_2 + 2H_2O \rightarrow Si(OH)_4$] led to release of Si species.[39] In comparison with PSi, BiM@PSi exhibited higher release of Si in this H_2O_2-triggered oxidation, indicating accelerated oxidation degree of PSi by AuNPs and AgNPs (Figure 2c). This phenomenon might be ascribed to the powerful electron transfer ability of AuNPs/AgNPs, which greatly improved the electron transition efficiency between PSi and H_2O_2 by providing multiple electron enrichment regions. The catalytic effect of metal nanoparticles is quite similar to that took place in metal-assisted chemical etching of Si.[41]

In the CQDs@PSi nanohybrid, the ratiometric fluorescence change can be observed as the oxidation of PSi by H_2O_2 decrease PSi's fluorescence and block FRET between PSi and CQDs. The formation of SiO_2 layer in H_2O_2 solution (100 μM, PBS) can be clearly seen by forming a loose structure in TEM images (Figure S8 in Supporting Information). To further confirm the mechanism, neat CQDs were also incubated with H_2O_2. Nevertheless, H_2O_2 exerts no significant effect on the FL intensity of the neat CQDs (Figure S9 in Supporting Information). Comparing to CQDs@PSi, the BiM-CQDs@PSi undergoes a quicker change in the ratiometric fluorescence when both of them are incubated in H_2O_2 aqueous. As shown in Figure 2d, the decrease rate of $I_{Si}/(I_{Si} + I_C)$ value is obviously faster for BiM-CQDs@PSi compared to CQDs@PSi, where I_{Si} and I_C refer to the FL peak intensity of PSi and CQDs, respectively. The results should be ascribed to the enhanced oxidation efficiency catalyzed by the bimetallic nanoparticles. In addition, the rate of fluorescence alternation from red to blue is in dependent on the concentration of H_2O_2. As shown in Figure 3, the higher the concentration of H_2O_2, the faster the change of ratiometric fluorescence color, indicating the potential for H_2O_2 analysis. Because the kinetics of PSi oxidation is directly related to the rate of ratiometric FL change, the promoted oxidation kinetics can thereby increase the sensitivity of FL response toward H_2O_2 stimuli.

Visual Response toward Glucose Based on H_2O_2 Generated by GOX-Catalyzed Oxidation of Glucose. The GOX-based catalytic system has been widely employed for the detection of glucose (Glu).[42] As illustrated in Figure 4a, enzymatic oxidation of glucose produces H_2O_2 and gluconic acid. Owing to fast ratiometric fluorescence change triggered

https://dx.doi.org/10.1021/acssensors.0c00718
ACS Sens. 2020, 5, 2096−2105

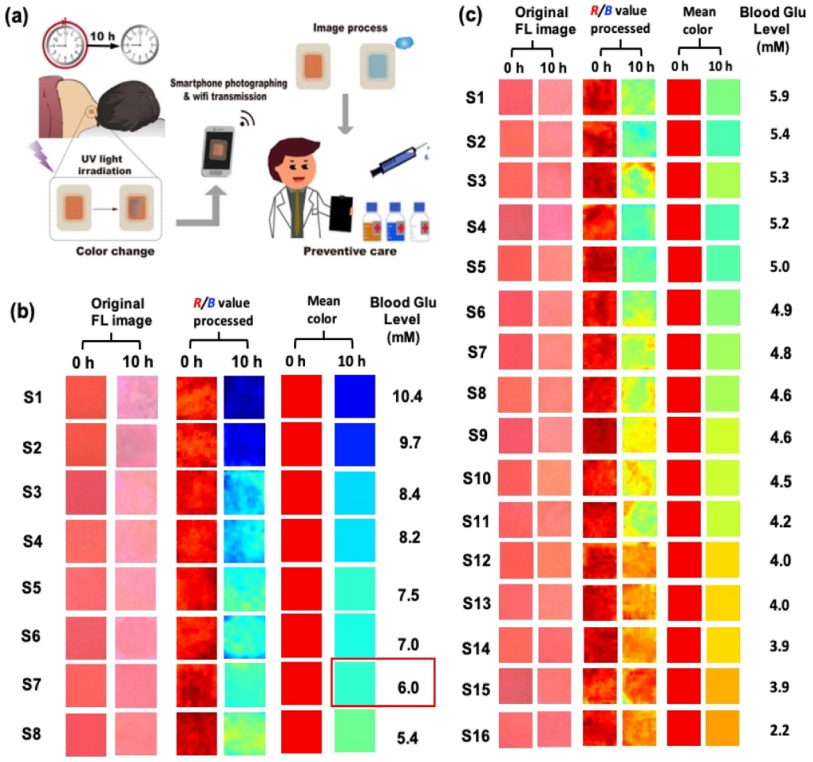

Figure 6. (a) Schematic illustration for noninvasive and visual monitoring of sweat glucose. Origin and processed FL photos of the wearable pad from diabetics (b) or health (c) volunteers.

by H_2O_2, BiM-CQDs@PSi could be utilized for analysis of glucose in the presence of GOX in simulated sweat. Obviously, the time required for complete blue fluorescence is shortened along with the increase of glucose concentration (Figure 4b) because of the improved H_2O_2 concentration at a high glucose level. Besides these visual results, the FL spectra of BiM-CQDs@PSi particles under different glucose levels furtherly confirmed that glucose can accelerate the ratiometric fluorescence transition in the GOX catalytic system. The transition rate of the fluorescence peak from red PSi to blue CQDs is faster as the concentration of glucose increases (Figure S10a−e in Supporting Information). And the value of $I_{Si}/(I_{Si} + I_C)$ in FL spectra decreases with the increased glucose level at each time (Figure S10f in Supporting Information). Compared with BiM-CQDs@PSi, time required for CQDs@PSi particles to completely turn blue is significantly longer (Figure S11 in Supporting Information), further confirming the acceleration of the oxidation process by bimetallic nanoparticles.

Cytotoxicity of BiM-CQDs@PSi. To verify the biocompatibility of BiM-CQDs@PSi, cytotoxicity experiment was conducted using two kinds of typical model cells for skin tissue, HaCaT and NIH3T3 cells. As shown in Figure S12 in Supporting Information, co-incubating of these cells with BiM-CQDs@PSi particles (0.1, 0.5, 1 mg/mL for 24 h or 48 h) led to more than 85% viabilities of NIH3T3 cells and 90% viabilities of HaCaT cells, indicating low cell toxicity and good biocompatibility. Thus, the material can be directly applied on skin surface with few side effects.

Construction of Wearable Pad and *In Vitro* Glucose Monitoring in Simulated Skin. To prepare wearable devices for skin-interfaced detection, BiM-CQDs@PSi particles and GOX were co-immobilized in the biopolymer film supported by the flexible and adhesive PU membrane (Tegaderm Film, 3M, USA). As illustrated in Figure 5a, CS cross-linked with GPTMS[43] was chosen as the biocompatible matrix to uniformly disperse BiM-CQDs@PSi particles and GOX because of its high biocompatibility, good film-forming characteristics, efficient encapsulation by polymer chains, and ability to maintain enzyme's activity.[44] Owing to merits of flexibility, adhesiveness and high biocompatibility, the as-prepared BiM-CQDs@PSi/GOX/CS/PU pad could be directly attached on skin.

To explore the potential of the obtained pad for monitoring of sweat glucose, *in vitro* glucose monitoring was conducted using cotton pad as the simulated skin. After the BiM-CQDs@PSi/GOX/CS/PU pad was patched on the cotton pad, simulated sweat (1 mL) containing different concentrations of glucose (0, 5, 7.5, 10, and 15 mM) was dropped on the back side of the cotton pad. Digital photos of the attached pad were taken every 4 h by the camera on a smartphone under UV irradiation (light emitting diode—LED, 377 nm). As shown in Figure 5b, the change of fluorescence color from red to blue within 10 h can be directly observed by naked eyes. In addition, the dynamics of this color change is closely related to glucose concentration. The higher the glucose concentration, the faster the blue color appears. Obviously, glucose facilitates red → blue change of BiM-CQDs@PSi, indicating that GOX keeps its enzyme activity in the CS film and the produced H_2O_2 in enzymatic oxidation of glucose promotes the oxidation process of PSi.

RGB analysis was utilized to quantitatively evaluate the glucose level in simulated sweat. After the intensity of the red or blue channel in the fluorescence image of BiM-CQDs@PSi/GOX/CS/PU pad was obtained through Photoshop CC software (Adobe Inc.), the ratiometric intensity value of the

https://dx.doi.org/10.1021/acssensors.0c00718
ACS Sens. 2020, 5, 2096−2105

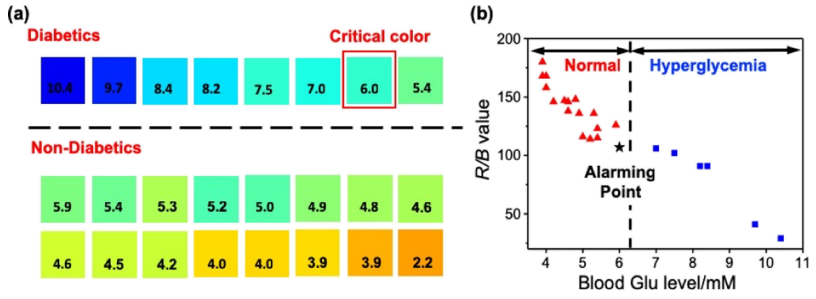

Figure 7. (a) Summary of the processed FL photo for each volunteer. Indicated number presents the fasting BG level tested by a commercial glucometer. (b) Distribution of R/B values with the fasting BG level.

red *versus* blue channel (R/B) was calculated. Figure 5c demonstrated the R/B value in the presence of different concentrations of glucose at different times. The higher change kinetics of ratiometric fluorescence at a higher glucose level could be easily revealed. In addition, this R/B value shows linear correlation with the concentration of glucose with a sensitivity of 3.46% mM^{-1}, indicating potential for quantitative analysis of glucose (Figure 5d). As BiM facilitated H_2O_2-triggered oxidation of PSi, the same *in vitro* experiment using CQDs@PSi/GOX/CS/PU needs much longer time for complete disappearance of PSi's red fluorescence and recovery of CQDs's blue fluorescence (Figure S13 in Supporting Information).

On-Body Monitoring of Sweat Glucose. In comparison with glucose detection by finger-pricked blood, noninvasive monitoring of glucose using accessible human biofluids provides potential for continuous, real-time, and out-of-clinic health monitoring. Amongst, noninvasive monitoring of glucose in sweat that is easily accessed with capability of continuous sampling is attractive because of the correlation of the glucose level between blood and sweat. However, direct monitoring of sweat glucose remains a great challenge because of its low concentration (~100 times lower than BG level). On the other hand, conventional sweat analysis involve collection using gauze pads taped to the skin, making on-site, real-time, and convenient detection not possible. The developed BiM-CQDs@PSi/GOX/CS/PU pad has possibility for on-body monitoring of sweat glucose by combination of key merits including flexibility, high biocompatibility, and glucose-sensitive ratiometric fluorescence.

As illustrated in Figure 6a, the BiM-CQDs@PSi/GOX/CS/PU pad was patched on the back-neck area of volunteers. Monitoring of sweat glucose was conducted on 8 diabetics (6 males and 2 females, aged from 52 to 85) and 16 healthy volunteers (12 males and 4 females, aged from 19 to 30) from the Zhejiang University Hospital. To minimize individual difference caused by lactic acid secretion during diet and exercise process, monitoring of sweat glucose was conducted during night sleep (10 h). This detection strategy can improve the detection accuracy and sensitivity owing to the accumulation and persistent secretion of glucose in sweat. On the one hand, bimetallic nanoparticles promote the oxidation of PSi by H_2O_2 generated in enzymatic oxidation of glucose, leading to a fast ratiometric fluorescence change. On the other hand, the accumulated sweat glucose in the detection process can further accelerate the ratiometric fluorescence change, thereby increasing the overall sensitivity. Digital photos of these wearable pads before and after detection were taken by the camera on a smartphone under UV irradiation (377 nm). It can be seen by the naked eye that red color in the fluorescence image of the pad reduces after detection. However, it is difficult to clearly distinguish different samples by naked eyes because of a slight change by the trace content of glucose in sweat. Thus, a simple color normalization method is employed. First, fluorescence images of each BiM-CQDs@PSi/GOX/CS/PU pad before and after detection were classified into one group (totally 24 samples). Second, intensity of the red or blue channel of each points was extracted and the R/B values were calculated. Then, the point with the maximum R/B value was colored by red and the point with the minimum R/B value was colored by blue; other points are colored between red and blue according to their R/B values. Finally, the mean value of normalized R/B values of each image was calculated to obtain an average color. Images with an averaged color were obtained after this procedure and applied in analysis (Figure 6b,c).

To distinguish people with the hypoglycemia state or normal BG, the image obtained from the volunteer with a BG level of 6.0 mM (tested by commercial blood glucometer), that is very close to the critical level between hypoglycemia and normal state (6.2 mM, S7), is settled as the critical color (Figure 6b). As glucose promote the change kinetics of ratiometric fluorescence from red to blue, a higher level of glucose leads to a higher degree of color change from red to blue. The resulted image for each detection is summarized in Figure 7. Hyperglycemia and normal BG level can be distinguished in comparison with the critical color. Besides the visual color, the calculated R/B values obtained by the hyperglycemia volunteer is lower than that obtained by the normal person. Thus, S1−S6 (Figure 6b) with a bluer image were under the hypoglycemia state, while S8 maintained a normal BG level during the detection process (under control of hypoglycemic drugs). At the same time, all health people had a normal BG level with much red images (S1−S18, Figure 6c). Diagnosis results for hyperglycemia patients by using the developed visualization method are consistent with that obtained through BG detection by a commercial blood glucometer, indicating potential for noninvasive, semiquantitative tracking of physiological status.

CONCLUSIONS

In summary, we have developed a platform for noninvasive and visual monitoring of sweat glucose based on glucose-sensitive ratiometric fluorescence nanohybrids. With different glucose levels in sweat, the oxidation of luminescent PSi by production of H_2O_2 through enzymatic oxidation of glucose could change the FRET effect between PSi and CQDs and decay PSi's red fluorescence, leading to visual fluorescence change from red

https://dx.doi.org/10.1021/acssensors.0c00718
ACS Sens. 2020, 5, 2096−2105

(PSi) to blue (CQDs). On body monitoring of sweat glucose using the proposed flexible pad demonstrates good resolution capacity between hyperglycemia and normal glucose state. This noninvasive and visual detection will be easy to operate if a smartphone integrates a miniature UV light source. Because the oxidation of PSi is irreversible, the patch is designed to be disposal in future application. As H_2O_2 is a well-known product in oxidoreductases, a universal platform to detect any substrates of oxidoreductases including a large variety of metabolites (*e.g.,* glucose, cholesterol, lactate, choline, L-lysine, pyruvate, glutamate, alcohol, xanthine, D-galactose, amino acids, sn-glycerol-3-phosphate, etc.) is possible. The specificity of the detection could be easily ensured by choice of the corresponding enzyme. To meet the requirements for different application purposes, the co-immobilized enzyme could be changed and the membrane to support the active detection layer can be further adjusted. In other words, the platform demonstrated here may be extended for visual detection of a variety of metabolites, and it is amenable for long-term home-based health management and treatment of metabolic diseases.

■ ASSOCIATED CONTENT

Supporting Information

The Supporting Information is available free of charge at https://pubs.acs.org/doi/10.1021/acssensors.0c00718.

More detailed characterization of PSi, BiM@PSi, CQDs, and CQDs@PSi; fluorescence property of AuNPs@PSi and AgNPs@PSi; cytotoxicity results of BiM-CQDs@PSi particles; and results of control experiments of CQDs@PSi particles (PDF)

■ AUTHOR INFORMATION

Corresponding Authors

Fengna Xi − *Institute of Analytical Chemistry, Department of Chemistry, Zhejiang University, Hangzhou 310058, China; Department of Chemistry, Zhejiang Sci-Tech University, Hangzhou 310018, China;* orcid.org/0000-0001-8564-8911; Email: Fengnaxi@zstu.edu.cn

Jianmin Wu − *Institute of Analytical Chemistry, Department of Chemistry, Zhejiang University, Hangzhou 310058, China;* orcid.org/0000-0002-0999-9194; Email: wjm-st1@zju.edu.cn

Authors

Yaoxuan Cui − *Institute of Analytical Chemistry, Department of Chemistry, Zhejiang University, Hangzhou 310058, China*

Wei Duan − *Institute of Analytical Chemistry, Department of Chemistry, Zhejiang University, Hangzhou 310058, China*

Yao Jin − *Institute of Analytical Chemistry, Department of Chemistry, Zhejiang University, Hangzhou 310058, China*

Fangjie Wo − *Institute of Analytical Chemistry, Department of Chemistry, Zhejiang University, Hangzhou 310058, China*

Complete contact information is available at: https://pubs.acs.org/10.1021/acssensors.0c00718

Author Contributions

The manuscript was written through contributions of all authors.

Notes

The authors declare no competing financial interest.

■ ACKNOWLEDGMENTS

We gratefully acknowledge clinical trial volunteers from the Zhejiang University Hospital. We acknowledge the financial support from National Natural Science Foundation of China (nos. 21275218, 21575127, and 21874118) and Hangzhou GSPMED Medical Appliances Co. Ltd.

■ REFERENCES

(1) Cho, N. H.; Shaw, J. E.; Karuranga, S.; Huang, Y.; da Rocha Fernandes, J. D.; Ohlrogge, A. W.; Malanda, B. IDF Diabetes Atlas: Global estimates of diabetes prevalence for 2017 and projections for 2045. *Diabetes Res. Clin. Pr.* **2018**, *138*, 271−281.

(2) Wild, S.; Roglic, G.; Green, A.; Sicree, R.; King, H. Global Prevalence of Diabetes: Estimates for the Year 2000 and Projections for 2030. *Diabetes Care* **2004**, *27*, 1047−1053.

(3) Gross, T. M.; Bode, B. W.; Einhorn, D.; Kayne, D. M.; Reed, J. H.; White, N. H.; Mastrototaro, J. J. Performance Evaluation of the Minimed Continuous Glucose Monitoring System During Patient Home Use. *Diabetes Technol. The.* **2000**, *2*, 49−56.

(4) Kim, J.; Campbell, A. S.; Wang, J. Wearable non-invasive epidermal glucose sensors: A review. *Talanta* **2018**, *177*, 163−170.

(5) Lin, Y.; Bariya, M.; Nyein, H. Y. Y.; Kivimäki, L.; Uusitalo, S.; Jansson, E.; Ji, W.; Yuan, Z.; Happonen, T.; Liedert, C.; Hiltunen, J.; Fan, Z.; Javey, A. Porous Enzymatic Membrane for Nanotextured Glucose Sweat Sensors with High Stability toward Reliable Non-invasive Health Monitoring. *Adv. Funct. Mater.* **2019**, *29*, 1902521.

(6) Lee, H.; Song, C.; Hong, Y. S.; Kim, M. S.; Cho, H. R.; Kang, T.; Shin, K.; Choi, S. H.; Hyeon, T.; Kim, D. H. Wearable/disposable sweat-based glucose monitoring device with multistage transdermal drug delivery module. *Sci. Adv.* **2017**, *3*, No. e1601314.

(7) Lee, H.; Choi, T. K.; Lee, Y. B.; Cho, H. R.; Ghaffari, R.; Wang, L.; Choi, H. J.; Chung, T. D.; Lu, N.; Hyeon, T.; Choi, S. H.; Kim, D.-H. A graphene-based electrochemical device with thermoresponsive microneedles for diabetes monitoring and therapy. *Nat. Nanotechnol.* **2016**, *11*, 566−572.

(8) Shibata, H.; Heo, Y. J.; Okitsu, T.; Matsunaga, Y.; Kawanishi, T.; Takeuchi, S. Injectable hydrogel microbeads for fluorescence based in vivo continuous glucose monitoring. *Proc. Natl. Acad. Sci.* **2010**, *107*, 17894−17898.

(9) Zhang, J.; Hodge, W.; Hutnick, C.; Wang, X. Noninvasive Diagnostic Devices for Diabetes through Measuring Tear Glucose. *J. Diabetes Sci. Technol.* **2011**, *5*, 166−172.

(10) Malik, S.; Khadgawat, R.; Anand, S.; Gupta, S. Non-invasive detection of fasting blood glucose level via electrochemical measurement of saliva. *SpringerPlus* **2016**, *5*, 701.

(11) Karim, M. N.; Anderson, S. R.; Singh, S.; Ramanathan, R.; Bansal, V. Nanostructured silver fabric as a free-standing nanoZyme for colorimetric detection of glucose in urine. *Biosens. Bioelectron.* **2018**, *110*, 8−15.

(12) Zierler, K. Whole body glucose metabolism. *Am. J. Physiol. Endocrinol. Metab.* **1999**, *276*, E409−E426.

(13) Moyer, J.; Wilson, D.; Finkelshtein, I.; Wong, B.; Potts, R. Correlation between Sweat Glucose and Blood Glucose in Subjects with Diabetes. *Diabetes Technol. The.* **2012**, *14*, 398−402.

(14) Rebrin, K.; Steil, G. M. Can Interstitial Glucose Assessment Replace Blood Glucose Measurements? *Diabetes Technol. The.* **2000**, *2*, 461−472.

(15) Panchbhai, A. S. Correlation of Salivary Glucose Level with Blood Glucose Level in Diabetes Mellitus. *J. Oral & Maxillofac.* **2012**, *3*, No. e3.

(16) Giardini, A.; Roberts, J. R. E. Concentration of Glucose and Total Chloride in Tears. *Br. J. Ophthalmol.* **1950**, *34*, 737−743.

(17) Gao, W.; Emaminejad, S.; Nyein, H. Y. Y.; Challa, S.; Chen, K.; Peck, A.; Fahad, H. M.; Ota, H.; Shiraki, H.; Kiriya, D.; Lien, D.-H.; Brooks, G. A.; Davis, R. W.; Javey, A. Fully integrated wearable sensor arrays for multiplexed in situ perspiration analysis. *Nature* **2016**, *529*, 509−514.

(18) Sonner, Z.; Wilder, E.; Heikenfeld, J.; Kasting, G.; Beyette, F.; Swaile, D.; Sherman, F.; Joyce, J.; Hagen, J.; Kelley-Loughnane, N.; Naik, R. The microfluidics of the eccrine sweat gland, including biomarker, transport, and biosensing implications. *Biomicrofluidics* **2015**, *9*, 031301.
(19) Koh, A.; Kang, D.; Xue, Y.; Lee, S.; Pielak, R. M.; Kim, J.; Hwang, T.; Min, S.; Banks, A.; Bastien, P.; Manco, M. C.; Wang, L.; Ammann, K. R.; Jang, K.-I.; Won, P.; Han, S.; Ghaffari, R.; Paik, U.; Slepian, M. J.; Balooch, G.; Huang, Y.; Rogers, J. A. A soft, wearable microfluidic device for the capture, storage, and colorimetric sensing of sweat. *Sci. Transl. Med.* **2016**, *8*, 366ra165.
(20) Heo, Y. J.; Shibata, H.; Okitsu, T.; Kawanishi, T.; Takeuchi, S. Long-term in vivo glucose monitoring using fluorescent hydrogel fibers. *Proc. Natl. Acad. Sci.* **2011**, *108*, 13399−13403.
(21) Mortellaro, M.; DeHennis, A. Performance characterization of an abiotic and fluorescent-based continuous glucose monitoring system in patients with type 1 diabetes. *Biosens. Bioelectron.* **2014**, *61*, 227−231.
(22) Schreml, S.; Meier, R. J.; Kirschbaum, M.; Kong, S. C.; Gehmert, S.; Felthaus, O.; Küchler, S.; Sharpe, J. R.; Wöltje, K.; Weiß, K. T.; Albert, M.; Seidl, U.; Schröder, T.; Morsczeck, C.; Prantl, L.; Duschl, C.; Pedersen, S. F.; Gosau, M.; Berneburg, M.; Wolfbeis, O. S.; Landthaler, M.; Babilas, P. Luminescent Dual Sensors Reveal Extracellular pH-Gradients and Hypoxia on Chronic Wounds That Disrupt Epidermal Repair. *Theranostics* **2014**, *4*, 721−735.
(23) Gao, X.; Ding, C.; Zhu, A.; Tian, Y. Carbon-Dot-Based Ratiometric Fluorescent Probe for Imaging and Biosensing of Superoxide Anion in Live Cells. *Anal. Chem.* **2014**, *86*, 7071−7078.
(24) Anglin, E.; Cheng, L.; Freeman, W.; Sailor, M. Porous silicon in drug delivery devices and materials. *Adv. Drug Deliv. Rev.* **2008**, *60*, 1266−1277.
(25) Chen, X.; Wo, F.; Jin, Y.; Tan, J.; Lai, Y.; Wu, J. Drug-Porous Silicon Dual Luminescent System for Monitoring and Inhibition of Wound Infection. *ACS Nano* **2017**, *11*, 7938−7949.
(26) Park, J.-H.; Gu, L.; von Maltzahn, G.; Ruoslahti, E.; Bhatia, S. N.; Sailor, M. J. Biodegradable luminescent porous silicon nanoparticles for in vivo applications. *Nat. Mater.* **2009**, *8*, 331−336.
(27) Tzur-Balter, A.; Shatsberg, Z.; Beckerman, M.; Segal, E.; Artzi, N. Mechanism of erosion of nanostructured porous silicon drug carriers in neoplastic tissues. *Nat. Commun.* **2015**, *6*, 6208.
(28) Massad-Ivanir, N.; Bhunia, S.; Jelinek, R.; Segal, E. Porous Silicon Bragg Reflector/Carbon Dot Hybrids: Synthesis, Nanostructure, and Optical Properties. *Front. Chem.* **2018**, *6*, 574.
(29) Massad-Ivanir, N.; Bhunia, S.; Raz, N.; Segal, E.; Jelinek, R. Synthesis and characterization of a nanostructured porous silicon/carbon dot-hybrid for orthogonal molecular detection. *NPG Asia Mater.* **2018**, *10*, No. e463.
(30) Dovzhenko, D.; Osipov, E.; Martynov, I.; Samokhvalov, P.; Eremin, I.; Kotkovskii, G.; Chistyakov, A. Porous Silicon Microcavity Modulates the Photoluminescence Spectra of Organic Polymers and Quantum Dots. *Mater. Today Proc.* **2016**, *3*, 485−490.
(31) Gaur, G.; Koktysh, S. D.; Weiss, M. S. Immobilization of Quantum Dots in Nanostructured Porous Silicon Films: Characterizations and Signal Amplification for Dual-Mode Optical Biosensing. *Adv. Funct. Mater.* **2013**, *23*, 3604−3614.
(32) Dovzhenko, D.; Osipov, E.; Martynov, I.; Linkov, P.; Linkov, A. Enhancement of Spontaneous Emission from CdSe/CdS /ZnS Quantum Dots at the Edge of the Photonic Band Gap in a Porous Silicon Bragg Mirror. *Phys. Proc.* **2015**, *73*, 126−130.
(33) Zhou, J.; Yang, Y.; Zhang, C.-Y. A low-temperature solid-phase method to synthesize highly fluorescent carbon nitride dots with tunable emission. *Chem. Commun.* **2013**, *49*, 8605−8607.
(34) Ji, X.; Song, X.; Li, J.; Bai, Y.; Yang, W.; Peng, X. Size Control of Gold Nanocrystals in Citrate Reduction: The Third Role of Citrate. *J. Am. Chem. Soc.* **2007**, *129*, 13939−13948.
(35) Montazer, M.; Allahyarzadeh, V. Electroless Plating of Silver Nanoparticles/Nanolayer on Polyester Fabric Using $AgNO_3$/NaoH and Ammonia. *Ind. Eng. Chem. Res.* **2013**, *52*, 8436−8444.
(36) Lehmann, V.; Gösele, U. Porous silicon formation: A quantum wire effect. *Appl. Phys. Lett.* **1991**, *58*, 856−858.
(37) Norman, T. J.; Grant, C. D.; Schwartzberg, A. M.; Zhang, J. Z. Structural correlations with shifts in the extended plasma resonance of gold nanoparticle aggregates. *Opt. Mater.* **2005**, *27*, 1197−1203.
(38) Daniel, L. S.; Nagai, H.; Sato, M. Absorption spectra and photocurrent densities of Ag nanoparticle/TiO_2 composite thin films with various amounts of Ag. *J. Mater. Sci.* **2013**, *48*, 7162−7170.
(39) Joo, J.; Cruz, J. F.; Vijayakumar, S.; Grondek, J.; Sailor, M. J. Photoluminescent Porous Si/SiO_2Core/Shell Nanoparticles Prepared by Borate Oxidation. *Adv. Funct. Mater.* **2014**, *24*, 5688−5694.
(40) Lakowicz, J. R.; Ray, K.; Chowdhury, M.; Szmacinski, H.; Fu, Y.; Zhang, J.; Nowaczyk, K. Plasmon-controlled fluorescence: a new paradigm in fluorescence spectroscopy. *Analyst* **2008**, *133*, 1308.
(41) Ghosh, R.; Imakita, K.; Fujii, M.; Giri, P. K. Effect of Ag/Au bilayer assisted etching on the strongly enhanced photoluminescence and visible light photocatalysis by Si nanowire arrays. *Phys. Chem. Chem. Phys.* **2016**, *18*, 7715−7727.
(42) Bruen, D.; Delaney, C.; Florea, L.; Diamond, D. Glucose Sensing for Diabetes Monitoring: Recent Developments. *Sensors* **2017**, *17*, 1866.
(43) Wu, J.; Sailor, M. J. Chitosan Hydrogel-Capped Porous SiO_2as a pH Responsive Nano-Valve for Triggered Release of Insulin. *Adv. Funct. Mater.* **2009**, *19*, 733−741.
(44) Lei, L.; Cao, Z.; Xie, Q.; Fu, Y.; Tan, Y.; Ma, M.; Yao, S. One-pot electrodeposition of 3-aminopropyltriethoxysilane-chitosan hybrid gel film to immobilize glucose oxidase for biosensing. *Sensor. Actuat. B-Chem.* **2011**, *157*, 282−289.

https://dx.doi.org/10.1021/acssensors.0c00718
ACS Sens. 2020, 5, 2096−2105